

Efficient Joint Precoding Design for Wideband Intelligent Reflecting Surface-Assisted Cell-Free Network

Yajun Wang, Jinghan Jiang, Xin Du, Zhuxian Lian, Qingqing Wu, *Senior Member, IEEE*, and Wen Chen, *Senior Member, IEEE*

Abstract—In this paper, we propose an efficient joint precoding design method to maximize the weighted sum-rate in wideband intelligent reflecting surface (IRS)-assisted cell-free networks by jointly optimizing the active beamforming of base stations and the passive beamforming of IRS. Due to employing wideband transmissions, the frequency selectivity of IRSs has to be taken into account, whose response usually follows a Lorentzian-like profile. To address the high-dimensional non-convex optimization problem, we employ a fractional programming approach to decouple the non-convex problem into subproblems for alternating optimization between active and passive beamforming. The active beamforming subproblem is addressed using the consensus alternating direction method of multipliers (CADMM) algorithm, while the passive beamforming subproblem is tackled using the accelerated projection gradient (APG) method and Fletcher-Reeves conjugate gradient method (FRCG). Simulation results demonstrate that our proposed approach achieves significant improvements in weighted sum-rate under various performance metrics compared to primal-dual subgradient (PDS) with ideal reflection matrix. This study provides valuable insights for computational complexity reduction and network capacity enhancement.

Index Terms—Intelligent reflecting surface (IRS), CADMM, APG, joint precoding.

I. INTRODUCTION

Ultra-dense networking technology (UDN) enhances network capacity by increasing the number of base stations (BSs) and utilizing small cells [1]. In traditional cellular networks, a BS typically serves all users within a cell, leading to significant interference for users at the cell boundaries from neighboring cells [2]. UDN addresses this issue by dividing the cell into smaller units through an increased number of BSs, thereby reducing the number of users per cell and improving network capacity and coverage. However, this approach also introduces challenges in terms of stronger inter-cell interference due to a higher BS density. Consequently, the potential improvement in

network capacity is limited as interference between adjacent cells increases.

The design concept of cell-free networks [3], [4] diverges from that of traditional cellular networks. Cell-free networks prioritize user-centricity, enabling seamless collaboration among all BSs without the constraints of cell boundaries. This enhanced flexibility in resource allocation optimizes signal transmission and fosters efficient BS cooperation, providing services to users in unrestricted areas. Consequently, this network design not only effectively mitigates inter-cell interference but also enhances network capacity. As a result, extensive research efforts have been dedicated to various aspects such as resource allocation [5], precoding/beamforming [6], and channel estimation [7].

In the current cell-free network [8], [9], increasing network capacity typically requires the addition of more distributed or small BSs, which presents challenges in terms of high power consumption and cost. However, as an emerging technology, intelligent reflective surfaces (IRSs) offer a viable alternative solution to address this problem [10], [11]. In recent years, IRS technology has garnered significant attention and has become a prominent research area. IRSs are usually metasurfaces, comprising numerous low-cost passive components. IRS can manipulate signal reflections by adjusting the phase and amplitude of each reflecting element [10]-[15]. This inherent flexibility enables IRS to alter transmission paths for signal focusing and orientation. Compared to the deployment of additional BSs, the integration of low-power IRS into cell-free networks can effectively modify the communication environment while minimizing the generation of heating noise [16]-[20]. Therefore, leveraging IRS as a potential solution allows for increased network capacity without relying on extensive deployment of distributed BSs.

IRSs have been extensively studied in various domains, including one-bit symbol-level precoding [21], energy efficiency [22], channel estimation [23], [24], and joint beamforming [25]-[29]. Some of these investigations focus on the use of IRS to enhance network capacity, particularly through the design of joint precoding. The researchers proposed an iterative algorithm that combines alternating optimization and penalty-based techniques to jointly optimize transmit beamforming at the BS and reflective beamforming at the IRS [30]. The objective is to minimize the total transmit power at the BS. In addition, passive beamforming and information transfer techniques in IRS-based multi-user multiple-

Yajun Wang, Jinghan Jiang, Xin Du and Zhuxian Lian are with the Department of Electronic Engineering, Jiangsu University of Science and Technology, Zhenjiang, 212003, China (e-mail: wangyj1859@just.edu.cn; 231112201113@stu.just.edu.cn; 211210301406@stu.just.edu.cn; zhuxianlian@just.edu.cn).

Qingqing Wu and Wen Chen are with the Department of Electronic Engineering, Shanghai Jiao Tong University, Shanghai, 200240, China, (e-mail: qingqingwu@sjtu.edu.cn; wenchen@sjtu.edu.cn).

This work was supported in part by FDCT under Grant 0119/2020/A3; in part by GDST under Grant 2020B1212030003; in part by STDF, Macau, under Grant 0036/2019/A1; in part by the National Key Project 2020YFB1807700 and Project 2018YFB1801102; and in part by NSFC under Grant 62001194, 61872184.

input multiple-output (MU-MIMO) systems were discussed in [31]. Furthermore, achievable rate maximization problems in spectrum-sharing MIMO systems have been addressed using a penalized dyadic decomposition-based gradient projection algorithm [32]. Moreover, researchers also addressed optimizations of energy efficiency and spectral efficiency of wireless communication aided by IRS as well as UAV networks [33]-[35]. Maximization of the minimum signal-to-interference-plus-noise ratio (SINR) in IRS-assisted multiple-input single-output (MISO) systems has been investigated to ensure fairness among users [36], [37]. Joint precoding problems involving multi-antenna, multi-BS, multi-IRS, multi-user, and multi-carrier scenarios were addressed in [38]. Furthermore, research works have explored various technologies combined with IRS, such as maximizing the signal-to-noise ratio (SNR) and designing hybrid beamforming for millimeter-wave (mmWave) communication systems assisted by IRS [39], [40], maximizing the sum-rate and power allocation in orthogonal frequency division multiplexing (OFDM) systems assisted by IRS [41], minimizing the total transmit power for radar communication assisted by IRS [42], and maximizing energy efficiency for hybrid active passive IRS-assisted energy efficient wireless communication [43]. Cooperative passive beamforming design was also investigated in double-IRS assisted multi-user MIMO systems [44], [45]. The channel model and performance prediction of double-IRS assisted communications were also analyzed in [46]. The design of beamforming for IRS-assisted cell-free massive MIMO communication systems was also addressed [47]-[50].

Nevertheless, the aforementioned studies on IRS-assisted communication systems have concentrated on narrowband systems, wherein the IRS is modeled as an adjustable phase shifter. In the context of wideband transmission, it is necessary to consider the frequency selective response of metamaterials. A frequency-dependent model for the amplitude and phase shift variations of the IRS elements has recently been proposed, and a weighted sum-rate maximization problem with OFDM modulations has been addressed [51], [52]. Nevertheless, the frequency response of a metamaterial typically exhibits a Lorentzian form [53]. While the application of metasurfaces in wideband communication systems has been recently explored as active massive MIMO antennas [54]-[56], there has been a paucity of research on passive metamaterial-based IRSs [57].

In this study, wideband IRS-assisted cell-free networks are investigated, wherein the frequency selective response of the IRS behaves a Lorentzian form. Our primary objective is to maximize the network capacity in wide-band scenarios for IRS-assisted cell-free networks. To achieve this, we address the problem of joint precoding design with the aim of maximizing the weighted sum-rate (WSR) across all users by optimizing active beamforming at the BSs and passive beamforming at the IRSs. While previous works [58]-[63], such as alternating optimization method (AO), prox-linear block coordinate descent (BCD), successive convex approximation (SCA) [58], alternating direction method of multipliers (ADMM) and iterative reflection coefficient updating (ICU) [59], also consider WSR maximization, they are specific cases

compared to our study. These previous methods primarily focus on scenarios involving a single BS and a single IRS, as well as narrowband communications.

The previous study [38] also investigated the maximization of the WSR in narrowband communications and proposed a primal-dual subgradient method (PDS) to address this problem. However, the PDS method involves iterative updates and lacks closed-form solutions for active precoding at BSs and passive precoding at IRSs, resulting in high computational complexity. Moreover, the PDS method only converges to a suboptimal solution, leaving room for further performance improvement. Motivated by these observations, we reexamine the WSR maximization problem in IRS-assisted cell-free networks with the objective of developing a low complexity algorithm that overcomes the limitations of PDS methods. This paper highlights the following main contributions.

- To address the formidable task of maximizing the WSR in non-convex optimization problems with high-dimensional variables, we employ a two-step approach. First, we leverage the Lagrangian dual transformation (LDT) and multidimensional complex quadratic transformation (MCQT) techniques proposed in [64], [65]. This technique effectively decouples the active precoding/beamforming at the BS and the passive precoding at the IRS, thereby simplifying the overall optimization problem. Subsequently, we utilize the consensus alternating direction method of multipliers (CADMM) algorithm [66], and the accelerated projection gradient (APG) method [67], [68], as well as Fletcher-Reeves conjugate gradient (FRCG) method to solve subproblems related to active beamforming and passive beamforming, respectively. By integrating Lagrange duality transformation, MCQT, CADMM algorithms, and APG-FRCG algorithms together, we can effectively handle both non-convexity and high-dimensionality inherent in WSR maximization problems. Finally, our combined algorithm is denoted as CADMM-APG-FRCG algorithm.

- A commonly employed approach to tackle the decoupling precoding problem involves transforming it into a quadratic constrained quadratic programming (QCQP) subproblem. However, solving each QCQP subproblem poses significant challenges. In contrast to the method proposed in [38], our CADMM-APG-FRCG algorithm addresses QCQP subproblems with multiple constraints by decomposing them into multiple QCQP problems, each having only one constraint (QCQP-1). This decomposition offers the advantage of optimally solving all QCQP-1 subproblems and obtaining a simple closed-form solution. Unlike conventional methods, our algorithm eliminates the need for exhaustive search of optimal Lagrange dual variables, thereby avoiding convex or non-convex optimization problems during iteration. This algorithm is easy and efficient to implement, ensuring the effectiveness and excellent performance throughout the optimization process.

- The complexity analysis reveals that the proposed CADMM-APG-FRCG algorithm exhibits lower computational complexity compared to the existing PDS algorithm. Furthermore, the simulation results demonstrate a significant improvement in the WSR performance in all indices when the CADMM-APG-FRCG algorithm is used instead of the

PDS method. These findings indicate that the CADMM-APG-FRCG algorithm effectively optimizes the objective function and yields higher WSR values.

The remaining sections of this paper are organized as follows. Section II discusses the system model of IRS-assisted cell-free networks and presents the corresponding expression for the WSR maximization problem. In Section III, an alternative optimization framework is presented to address this problem. Section IV introduces the CADMM-APG-FRCG algorithm used for active and passive precoding. Simulations in Section V validate the performance of the presented CADMM-APG-FRCG algorithm for IRS-assisted cell-free networks. Finally, a conclusion is drawn in Section VI.

Notations: \mathbb{R} and \mathbb{C} denote sets of real and complex numbers, respectively; $[\cdot]^H$, $[\cdot]^T$, $[\cdot]^{-1}$, and $[\cdot]^*$ represent the conjugate-transpose, transpose, inverse, and conjugate operations, respectively; $[\mathbf{c}]_j$ is the j -th element of the vector \mathbf{c} ; $[\mathbf{B}]_{a,b}$ is the element in the b -th column and the a -th row of the matrix \mathbf{B} ; $E[\cdot]$ is the expectation operator; $\|\mathbf{c}\|$ denotes the Euclidean norm of its argument; $diag(\cdot)$ denotes the diagonal operation; $\Re\{\cdot\}$ denotes the real part of its argument; \otimes denotes the Kronecker product; $\mathbf{0}_M$ stands for an $M \times M$ zero matrix. \mathbf{I}_M denotes an $M \times M$ identity matrix. \mathbf{e}_m denotes a primary vector with 1 at the m -th location, and $\mathbf{1}_M$ is an M -length vector with elements being 1. A circularly symmetric complex Gaussian random vector \mathbf{c} with mean $\mathbf{0}$ and covariance matrix $\mathbf{\Pi}$ is denoted by $\mathbf{c} \sim \mathcal{CN}(\mathbf{0}, \mathbf{\Pi})$.

II. SYSTEM MODEL AND PROBLEM FORMULATION

A. System Model

The main focus of this paper is to investigate a wideband cell-free network system that utilizes distributed BSs and IRSs to collectively serve a group of users, as shown in Fig. 1. The system consists of N_b BSs, N_c IRSs, M subcarriers, and K users with multiple antennas. To facilitate the analysis, we make certain assumptions. Each BS is equipped with N_t antennas, each user has N_r antennas, and each IRS is comprised of R reflection units. We represent the index sets for the BSs, users, IRSs, subcarriers, and IRS elements as $\mathcal{N}_B = \{1, \dots, N_b\}$, $\mathcal{K} = \{1, \dots, K\}$, $\mathcal{N}_C = \{1, \dots, N_c\}$, $\mathcal{M} = \{1, \dots, M\}$, and $\mathcal{R} = \{1, \dots, R\}$, respectively.

1) Transmit Waveform Design:

Let $\mathbf{s}_{n_b,m} = [s_{n_b,m,1}, \dots, s_{n_b,m,K}]^T \in \mathbb{C}^K$, where $s_{n_b,m,k}$ represents the frequency domain symbol sent to the k -th user on the m -th subcarrier/tone from the n_b -th BS, $\mathbf{s}_{n_b,m} \sim \mathcal{CN}(\mathbf{0}_K, \mathbf{I}_K), \forall n_b \in \mathcal{N}_B, \forall m \in \mathcal{M}$. The precoded signal $\mathbf{x}_{n_b,m}$ at the n_b -th BS on the m -th subcarrier is given by

$$\mathbf{x}_{n_b,m} = \sum_{j=1}^K \mathbf{w}_{n_b,m,j} s_{n_b,m,j}, \quad (1)$$

where $\mathbf{w}_{n_b,m,j} \in \mathbb{C}^{N_t}$ is the precoding vector at the n_b -th BS in the downlink.

Firstly, the precoded signal $\{\mathbf{x}_{n_b,m}\}_{m=1}^M$ on all M tones at the n_b -th BS is transformed into the time domain using inverse discrete Fourier transform (IDFT). Subsequently, a

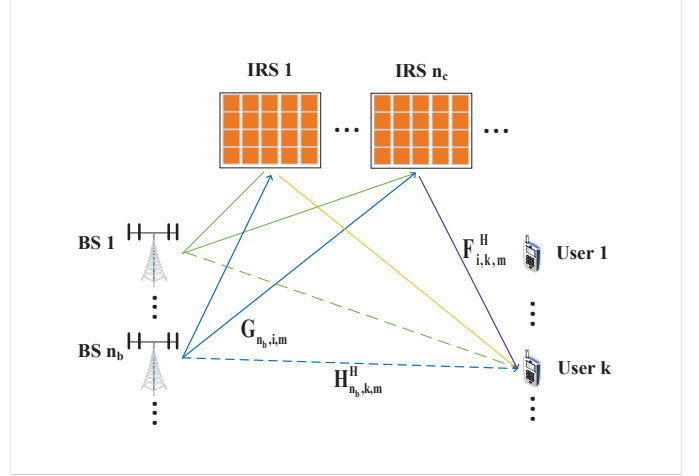


Fig. 1: The downlink channels in the IRS-aided cell-free network.

cyclic prefix (CP) is added to the time-domain signals before converting them from the N_t RF chain of the n_b -th BS to the radio frequency (RF) domain.

2) Channel Model:

In the presented IRS-assisted cell-free network, the channel between each BS and each user is composed of three parts: a BS-user link, N_c BS-IRS link, and N_c IRS-user link. Consequently, the equivalent channel $\mathbf{h}_{n_b,k,m}^H \in \mathbb{C}^{N_r \times N_t}$ between the n_b -th BS and the k -th user on the m -th tone can be expressed as follows.

$$\hat{\mathbf{H}}_{n_b,k,m}^H = \mathbf{H}_{n_b,k,m}^H + \sum_{i=1}^{N_c} \mathbf{F}_{i,k,m}^H \mathbf{\Phi}_{i,m}^H \mathbf{G}_{n_b,i,m}, \quad (2)$$

where $\mathbf{H}_{n_b,k,m}^H \in \mathbb{C}^{N_r \times N_t}$, $\mathbf{G}_{n_b,i,m} \in \mathbb{C}^{R \times N_t}$, $\mathbf{F}_{i,k,m}^H \in \mathbb{C}^{N_r \times R}$ represent the frequency domain channels on the m -th tone from the n_b -th BS to the k -th user, from the n_b -th BS to the i -th IRS, and from the i -th IRS to the k -th user, respectively. $\mathbf{\Phi}_{i,m} \in \mathbb{C}^{R \times R}$ is the reflection matrix at the i -th IRS on the m -th tone, which is given by

$$\mathbf{\Phi}_{i,m} = diag(\phi_{i,1,m}, \dots, \phi_{i,R,m}), \forall i \in \mathcal{N}_C, \quad (3)$$

where $\phi_{i,r,m}$ is the reflection coefficient (RC) of the r -th element at the i -th IRS for the m -th tone. Different from the ideal model [38], we employ the metamaterial-based IRS model discussed in [53], i.e., $\phi_{i,r,m}$ is modeled as a polarized dipole, and follow the following Lorentzian form.

$$\phi_{i,r,m} = \frac{\varphi_{i,r} f_m^2}{\psi_{i,r}^2 - f_m^2 + j\kappa_{i,r} f_m}, \quad (4)$$

$$\forall i \in \mathcal{N}_C, \forall r \in \mathcal{R}, \forall m \in \mathcal{M},$$

where $\varphi_{i,r} > 0$, $\psi_{i,r} > 0$, and $\kappa_{i,r}$ are the element-dependent oscillator strength, resonance frequency, and damping factor, respectively. These parameters can be tuned by external control for each element individually.

For the MIMO-OFDM system with bandwidth B , the central frequency of each subcarrier f_m is defined as $f_m = f_c + (m - \frac{M+1}{2}) \frac{B}{M}, \forall m \in \mathcal{M}$.

After CP is eliminated and the discrete Fourier transform (DFT) is applied, the transmitted signal is converted back to

the frequency domain symbol. Let $\mathbf{y}_{n_b,k,m} \in \mathbb{C}^{N_r}$ denote the baseband frequency domain signal on the tone m from the BS n_b to the user k . Based on the aforementioned channel model, $\mathbf{y}_{n_b,k,m}$ can be expressed as follows.

$$\begin{aligned} \mathbf{y}_{n_b,k,m} &= \hat{\mathbf{H}}_{n_b,k,m}^H \mathbf{x}_{n_b,m} \\ &= \left(\mathbf{H}_{n_b,k,m}^H + \sum_{i=1}^{N_c} \mathbf{F}_{i,k,m}^H \Phi_{i,m}^H \mathbf{G}_{n_b,i,m} \right) \sum_{j=1}^K \mathbf{w}_{n_b,m,j} s_{n_b,m,j}. \end{aligned} \quad (5)$$

B. Problem Formulation

Taking into account the transmit power constraints of the BS and RC constraints at the IRS, we investigate the problem of maximizing WSR in the IRS-assisted cell-free network presented. Define $\mathbf{F}_{k,m} = [\mathbf{F}_{1,k,m}^T, \dots, \mathbf{F}_{N_c,k,m}^T]^T$, $\mathbf{G}_{n_b,m} = [\mathbf{G}_{n_b,1,m}^T, \dots, \mathbf{G}_{n_b,N_c,m}^T]^T$, $\hat{\mathbf{H}}_{k,m} = [\hat{\mathbf{H}}_{1,k,m}^T, \dots, \hat{\mathbf{H}}_{N_b,k,m}^T]^T$, $\Phi_m = \text{diag}(\Phi_{1,m}, \dots, \Phi_{N_c,m})$, and $\mathbf{w}_{m,k} = [\mathbf{w}_{1,m,k}^T, \dots, \mathbf{w}_{N_b,m,k}^T]^T$, $\mathbf{s}_{m,k} = [s_{1,m,k}, \dots, s_{N_b,m,k}]^T$, the received signal $\mathbf{y}_{k,m} \in \mathbb{C}^{N_r}$ from the user k on the tone m is given by

$$\begin{aligned} \mathbf{y}_{k,m} &= \sum_{n_b=1}^{N_b} \sum_{j=1}^K (\mathbf{H}_{n_b,m,k}^H + \mathbf{F}_{k,m}^H \Phi_m^H \mathbf{G}_{n_b,m}) \mathbf{w}_{n_b,m,j} s_{n_b,m,j} + \mathbf{n}_{k,m} \\ &= \sum_{j=1}^K \hat{\mathbf{H}}_{k,m}^H \mathbf{w}_{m,j} s_{m,j} + \mathbf{n}_{k,m}, \end{aligned} \quad (6)$$

where $\mathbf{n}_{k,m} \triangleq [n_{k,m,1}^T, \dots, n_{k,m,N_r}^T]^T$ stands for additive white Gauss noise (AWGN), $\mathbf{n}_{k,m} \sim \mathcal{CN}(\mathbf{0}_{N_r}, \sigma^2 \mathbf{I}_{N_r})$, $\forall k \in \mathcal{K}, \forall m \in \mathcal{M}$.

Based on the channel estimation techniques proposed in [23], [24], we assume that all channel state information (CSI) can be accurately acquired in this study.

Then, the SINR of the transmit symbol $s_{k,m}$ at the k -th user on the m -th subcarrier is formulated as follows.

$$\begin{aligned} \gamma_{k,m} &= \mathbf{w}_{m,k}^H \hat{\mathbf{H}}_{k,m} \left(\sum_{j=1, j \neq k}^K \hat{\mathbf{H}}_{k,m}^H \mathbf{w}_{m,j} (\hat{\mathbf{H}}_{k,m}^H \mathbf{w}_{m,j})^H + \Xi_{k,m} \right)^{-1} \\ &\quad \times \hat{\mathbf{H}}_{k,m}^H \mathbf{w}_{m,k}, \end{aligned} \quad (7)$$

where $\Xi_{k,m} = \sigma^2 \mathbf{I}_{N_r}$ is a covariance matrix of $\mathbf{n}_{k,m}$.

The WSR for all K users can thus be expressed as follows.

$$R_{sum} = \sum_{k=1}^K \sum_{m=1}^M \xi_{k,m} \log_2(1 + \gamma_{k,m}), \quad (8)$$

where $\xi_{k,m} > 0$ is the weight factor of the k -th user on the m -th subcarrier.

Hence, the WSR maximization optimization problem can be expressed as

$$\mathcal{P}(0) : \max_{\mathbf{W}, \Phi} R_{sum}(\mathbf{W}, \Phi) = \sum_{k=1}^K \sum_{m=1}^M \xi_{k,m} \log_2(1 + \gamma_{k,m}) \quad (9a)$$

$$\text{s.t.} \quad \sum_{k=1}^K \sum_{m=1}^M \|\mathbf{w}_{n_b,m,k}\|^2 \leq P_{n_b, \max}, \forall n_b \in \mathcal{N}_{\mathcal{B}}, \quad (9b)$$

$$\phi_{i,r,m} \in \Omega, \quad (9c)$$

$$|\phi_{i,r,m}| \leq 1, \forall i \in \mathcal{N}_{\mathcal{C}}, \forall r \in \mathcal{R}, \forall m \in \mathcal{M}. \quad (9d)$$

where $P_{n_b, \max}$ represents the maximum transmit power of the n_b -th BS, Ω is the set of all $\phi_{i,r,m}$ satisfying equations (4). $\Phi \in \mathbb{C}^{MRN_c \times MRN_c}$ and $\mathbf{W} \in \mathbb{C}^{N_t N_b M K \times 1}$ is defined as follows, respectively.

$$\Phi = \text{diag}(\Phi_1, \dots, \Phi_2, \dots, \Phi_M),$$

$$\mathbf{W} = [\mathbf{w}_{1,1}^T, \mathbf{w}_{1,2}^T, \dots, \mathbf{w}_{1,K}^T, \mathbf{w}_{2,1}^T, \mathbf{w}_{2,2}^T, \dots, \mathbf{w}_{M,K}^T]^T. \quad (10)$$

The problem $\mathcal{P}(0)$ is a challenging high-dimensional non-convex optimization problem due to the deep coupling of variables in the objective function and the non-convex nature of the unit-modulus constraint. In the next section, we employ the LDT and the MCQT from [64], [65] to decouple \mathbf{W} and Φ . Subsequently, we propose the CADMM-APG-FRCG algorithm to achieve an optimal solution to each subproblem within joint optimization.

III. PROPOSED SOLUTION

In this section, we propose a simple and efficient approach to address the WSR optimization problem $\mathcal{P}(0)$ in (9). Firstly, we employ the LDT and MCQT from [64], [65] to convert $\mathcal{P}(0)$ into $\mathcal{P}(1)$, thereby decoupling the variables \mathbf{W} and Φ in the objective function into tractable subproblems discussed in Subsection III – A. Subsequently, we present a low-complexity algorithm to solve joint precoding design problems concerning \mathbf{W} and Φ , respectively, which leverages the CADMM-APG-FRCG algorithm [66]-[68].

A. Lagrangian Dual Transform

To address the complex sum-of-logarithms-of-ratio problem in the WSR maximization problem $\mathcal{P}(0)$ in (9), we employ the LDT to decouple the logarithms. Let us introduce an auxiliary variable $\boldsymbol{\eta} \in \mathbb{R}^{MK}$ with $\boldsymbol{\eta} = [\eta_{1,1}, \eta_{1,2}, \dots, \eta_{1,K}, \eta_{2,1}, \eta_{2,2}, \dots, \eta_{M,K}]^T$. Consequently, the problem $\mathcal{P}(0)$ is transformed into $\mathcal{P}(1)$.

$$\begin{aligned} \mathcal{P}(1) : \max_{\mathbf{W}, \Phi, \boldsymbol{\eta}} f(\mathbf{W}, \Phi, \boldsymbol{\eta}) \\ \text{s.t.} \quad (9b), (9c), (9d). \end{aligned} \quad (11)$$

where $f(\mathbf{W}, \Phi, \eta)$ is denoted by

$$\begin{aligned} f(\mathbf{W}, \Phi, \eta) &= \sum_{k=1}^K \sum_{m=1}^M \xi_{k,m} \log_2(1 + \eta_{k,m}) \\ &- \sum_{k=1}^K \sum_{m=1}^M \xi_{k,m} \eta_{k,m} + \sum_{k=1}^K \sum_{m=1}^M \xi_{k,m} (1 + \eta_{k,m}) f_{k,m}(\mathbf{W}, \Phi), \end{aligned} \quad (12)$$

where $f_{k,m}(\mathbf{W}, \Phi)$ is defined as

$$\begin{aligned} f_{k,m}(\mathbf{W}, \Phi) &= \\ &\mathbf{w}_{m,k}^H \hat{\mathbf{H}}_{k,m} \left(\sum_{j=1}^K \hat{\mathbf{H}}_{k,m}^H \mathbf{w}_{m,j} \left(\hat{\mathbf{H}}_{k,m}^H \mathbf{w}_{m,j} \right)^H + \Xi_{k,m} \right)^{-1} \\ &\times \hat{\mathbf{H}}_{k,m}^H \mathbf{w}_{m,k}, \end{aligned} \quad (13)$$

Then, the CADMM-APG-FRCG algorithm is devised to alternatively solve the variables η , \mathbf{W} and Φ .

B. Fix (\mathbf{W}, Φ) and solve η^{opt}

When (\mathbf{W}^*, Φ^*) remains unchanged, the optimal solution η in (12) is obtained by setting $\partial f / \partial \eta_{k,m} = 0$.

$$\eta_{k,m}^{\text{opt}} = \gamma_{k,m}^*, \forall k \in \mathcal{K}, \forall m \in \mathcal{M}. \quad (14)$$

By substituting $\eta_{k,m}^{\text{opt}} = \gamma_{k,m}^*$ (14) into (12), we can observe that only the final term in (12) depends on both variables Φ and \mathbf{W} . Thus, we can simplify (11) as optimization problems for Φ and \mathbf{W} .

C. Fix (Φ, η) and solve \mathbf{W}^{opt}

Given (Φ^*, η^*) , $\mathcal{P}(1)$ is equivalent to the following $\mathcal{P}(2)$.

$$\begin{aligned} \mathcal{P}(2) : \max_{\mathbf{W}} \quad & f_1(\mathbf{W}) = \sum_{k=1}^K \sum_{m=1}^M \zeta_{k,m} f_{k,m}(\mathbf{W}, \Phi^*) \\ \text{s.t.} \quad & \sum_{k=1}^K \sum_{m=1}^M \|\mathbf{w}_{n_b, m, k}\|^2 \leq P_{n_b, \max}, \forall n_b \in \mathcal{N}_{\mathcal{B}}, \end{aligned} \quad (15)$$

where $\zeta_{k,m} = \xi_{k,m} (1 + \eta_{k,m}^*)$. Since $f_{k,m}(\mathbf{W}, \Phi^*)$ in (15) represents a complex sum-of-fractions problem that is non-convex, the direct solution of (15) becomes highly challenging. To address this issue, we employ the MCQT, as presented in [64], by introducing auxiliary variables $\delta_{m,k} \in \mathbb{C}^{N_r}$ with $\delta = [\delta_{1,1}, \delta_{1,2}, \dots, \delta_{1,K}, \delta_{2,1}, \delta_{2,2}, \dots, \delta_{M,K}]$. Consequently, the $\mathcal{P}(2)$ is reformulated as

$$\begin{aligned} \max_{\mathbf{W}, \delta} \quad & f_2(\mathbf{W}, \delta) = \sum_{k=1}^K \sum_{m=1}^M 2\sqrt{\zeta_{k,m}} \Re\{\delta_{k,m}^H \hat{\mathbf{H}}_{k,m}^H \mathbf{w}_{m,k}\} \\ & - \sum_{k=1}^K \sum_{m=1}^M \delta_{k,m}^H \\ & \times \left(\sum_{j=1}^K \hat{\mathbf{H}}_{k,m}^H \mathbf{w}_{m,j} \left(\hat{\mathbf{H}}_{k,m}^H \mathbf{w}_{m,j} \right)^H + \Xi_{k,m} \right) \delta_{k,m} \\ \text{s.t.} \quad & \sum_{k=1}^K \sum_{m=1}^M \|\mathbf{w}_{n_b, m, k}\|^2 \leq P_{n_b, \max}, \forall n_b \in \mathcal{N}_{\mathcal{B}}. \end{aligned} \quad (16)$$

According to (16), solving \mathbf{W} in $\mathcal{P}(2)$ is equivalent to an alternative updating of δ and \mathbf{W} in (16), which will be addressed separately below.

C1. Fix \mathbf{W} and Solve δ^{opt}

Fixing \mathbf{W} in f_2 , and setting $\partial f_2 / \partial \delta_{k,m} = 0$, we can obtain the optimal solution for δ .

$$\begin{aligned} \delta_{k,m}^{\text{opt}} &= \sqrt{\zeta_{k,m}} \left(\sum_{j=1}^K \hat{\mathbf{H}}_{k,m}^H \mathbf{w}_{m,j} \left(\hat{\mathbf{H}}_{k,m}^H \mathbf{w}_{m,j} \right)^H + \Xi_{k,m} \right)^{-1} \\ &\times \hat{\mathbf{H}}_{k,m}^H \mathbf{w}_{m,k}. \end{aligned} \quad (17)$$

C2. Fix δ and Solve \mathbf{W}^{opt}

The optimal value δ obtained in (17) is substituted into f_2 , resulting in f_2 being solely associated with the variable \mathbf{W} . Define

$$\mathbf{d}_m = \sum_{k=1}^K \hat{\mathbf{H}}_{k,m} \delta_{k,m} \delta_{k,m}^H \hat{\mathbf{H}}_{k,m}^H, \quad (18a)$$

$$\mathbf{D}_m = \mathbf{I}_K \otimes \mathbf{d}_m, \mathbf{c}_{k,m} = \hat{\mathbf{H}}_{k,m} \delta_{k,m}. \quad (18b)$$

Then f_2 can be reformulated as

$$f_2(\mathbf{W}) = -\mathbf{W}^H \mathbf{D} \mathbf{W} + \Re\{2\mathbf{C}^H \mathbf{W}\} - U, \quad (19)$$

where

$$\mathbf{D} = \text{diag}(\mathbf{D}_1, \dots, \mathbf{D}_M), U = \sum_{k=1}^K \sum_{m=1}^M \delta_{k,m}^H \Xi_{k,m} \delta_{k,m}, \quad (20a)$$

$$\mathbf{C} = [\mathbf{c}_{1,1}^T, \mathbf{c}_{1,2}^T, \dots, \mathbf{c}_{1,K}^T, \mathbf{c}_{2,1}^T, \mathbf{c}_{2,2}^T, \dots, \mathbf{c}_{M,K}^T]^T. \quad (20b)$$

The f_2 in (16) can be simplified further.

$$\begin{aligned} \mathcal{P}(3) : \min_{\mathbf{W}} \quad & f_3(\mathbf{W}) = \mathbf{W}^H \mathbf{D} \mathbf{W} - \Re\{2\mathbf{C}^H \mathbf{W}\} \\ \text{s.t.} \quad & \mathbf{W}^H \mathbf{P}_{n_b} \mathbf{W} \leq P_{n_b, \max}, \forall n_b \in \mathcal{N}_{\mathcal{B}}, \end{aligned} \quad (21)$$

where $\mathbf{P}_{n_b} = \mathbf{I}_{MK} \otimes \{(\mathbf{e}_{n_b} \mathbf{e}_{n_b}^H) \otimes \mathbf{I}_{N_t}\}$, $\mathbf{e}_{n_b} \in \mathbb{R}^{N_b}$. The matrices \mathbf{D} and \mathbf{P}_{n_b} , $\forall n_b \in \mathcal{N}_{\mathcal{B}}$ being positive semidefinite, $\mathcal{P}(3)$ in (21) can be classified as a standard QCQP problem, which is generally known to be NP-hard. We employ the CADMM to optimally solve the QCQP.

C3. CADMM algorithm to solve \mathbf{W}

We employ CADMM to solve the subproblem of active beamforming (21). CADMM is derived from ADMM [69], [70]. To reduce computational complexity and address the challenging subproblems of ADMM, a consistency strategy known as CADMM is utilized [66]. Both ADMM and CADMM have been extensively applied in addressing convex and non-convex optimization problems [66], [69], [70]. For a complete understanding and practical application of ADMM and CADMM, readers can refer to the literature [66], [69], [70].

Let $\mathbf{V}_{n_b} = \mathbf{W}$, and \mathbf{V}_{n_b} be an auxiliary variable. Then $\mathcal{P}(3)$ can be equivalently formulated as follows.

$$\begin{aligned} \mathcal{P}(3') : \min_{\mathbf{W}} \quad & f_3(\mathbf{W}) \\ \text{s.t.} \quad & \mathbf{W} = \mathbf{V}_{n_b}, \end{aligned} \quad (22a)$$

$$\mathbf{V}_{n_b}^H \mathbf{P}_{n_b} \mathbf{V}_{n_b} \leq P_{n_b, \max}, \forall n_b \in \mathcal{N}_{\mathcal{B}}. \quad (22b)$$

The augmented Lagrangian function of $\mathcal{P}(3')$ is

$$L_\alpha(\mathbf{W}, \mathbf{V}_{n_b}, \mathbf{q}_{n_b}) = \mathbf{W}^H \mathbf{D} \mathbf{W} - \Re\{2\mathbf{C}^H \mathbf{W}\} + \alpha \sum_{n_b=1}^{N_b} \|\mathbf{W} - \mathbf{V}_{n_b} + \mathbf{q}_{n_b}\|^2, \quad (23)$$

where $\alpha > 0$ is a penalty parameter. \mathbf{q}_{n_b} represents the Lagrange dual vector. The CADMM method is employed to solve $\mathcal{P}(3')$, which follows an iterative form.

$$\mathbf{W}^{j+1} = \arg \min_{\mathbf{W}} L_\alpha(\mathbf{W}, \mathbf{V}_{n_b}^j, \mathbf{q}_{n_b}^j), \quad (24a)$$

$$\mathbf{V}_{n_b}^{j+1} = \arg \min_{\mathbf{V}} L_\alpha(\mathbf{W}^j, \mathbf{V}_{n_b}, \mathbf{q}_{n_b}^j), \quad (24b)$$

$$\mathbf{q}_{n_b}^{j+1} = \mathbf{q}_{n_b}^j + \mathbf{W}^{j+1} - \mathbf{V}_{n_b}^{j+1}, \forall n_b \in \mathcal{N}_{\mathcal{B}}. \quad (24c)$$

1) Solving \mathbf{W} in (24a):

To avoid the computational burden associated with directly solving (24a), which requires inverting a high-dimensional matrix \mathbf{D} of size $N_b N_t M K$, we employ a linearization strategy to address the quadratic term $\mathbf{W}^H \mathbf{D} \mathbf{W}$.

Specifically, we perform a first-order Taylor expansion of $\mathbf{W}^H \mathbf{D} \mathbf{W}$ at any given point \mathbf{W}_0 , then

$$\mathbf{W}^H \mathbf{D} \mathbf{W} = \mathbf{W}_0^H \mathbf{D} \mathbf{W}_0 + \Re\{2\mathbf{D} \mathbf{W}_0 (\mathbf{W} - \mathbf{W}_0)\} + \beta \|\mathbf{W} - \mathbf{W}_0\|^2, \quad (25)$$

where $\beta > 0$ is a penalty parameter. (24a) is equivalent to solving the following problem.

$$\min_{\mathbf{W}} \Re\{2\mathbf{D} \mathbf{W}_0 (\mathbf{W} - \mathbf{W}_0)\} + \beta \|\mathbf{W} - \mathbf{W}_0\|^2 - \Re\{2\mathbf{C}^H \mathbf{W}\} + \alpha \sum_{n_b=1}^{N_b} \|\mathbf{W} - \mathbf{V}_{n_b}^j + \mathbf{q}_{n_b}^j\|^2 \quad (26)$$

The derivative of the objective function with respect to \mathbf{W} is set to zero, yielding

$$\mathbf{W}^{j+1} = \frac{1}{N_b \alpha + \beta} \left[\beta \mathbf{W}_0 + \mathbf{C} - \mathbf{D} \mathbf{W}_0 + \alpha \sum_{n_b=1}^{N_b} (\mathbf{V}_{n_b}^j - \mathbf{q}_{n_b}^j) \right]. \quad (27)$$

2) Solving \mathbf{V}_{n_b} in (24b):

(24b) requires one to address the following optimization issue.

$$\min_{\mathbf{V}_{n_b}} \sum_{n_b=1}^{N_b} \|\mathbf{W}^{j+1} - \mathbf{V}_{n_b} + \mathbf{q}_{n_b}^j\|^2 \quad (28)$$

s.t. $\mathbf{V}_{n_b}^H \mathbf{P}_{n_b} \mathbf{V}_{n_b} \leq P_{n_b, \max}, \forall n_b \in \mathcal{N}_{\mathcal{B}}.$

Problem (28) is a QCQP with N_b constraints, which is generally known to be NP-hard. However, considering the special characteristics of this problem, we can equivalently transform it into N_b QCQPs with only one constraint each (QCQP-1), thereby enabling an optimal solution.

Based on the definition of \mathbf{P}_{n_b} , which is a 0-1 matrix, and (28) is equivalent to the following N_b QCQP-1.

$$\min_{\mathbf{V}_{n_b}} \|\mathbf{W}^{j+1} - \mathbf{V}_{n_b} + \mathbf{q}_{n_b}^j\|^2 \quad (29)$$

s.t. $\mathbf{V}_{n_b}^H \mathbf{V}_{n_b} \leq P_{n_b, \max}.$

Let $\epsilon_{n_b}^j = \mathbf{W}^{j+1} + \mathbf{q}_{n_b}^j$, the Lagrange function of (29) is

$$L_{\sigma_{n_b}}(\mathbf{V}_{n_b}, \sigma_{n_b}) = \|\mathbf{V}_{n_b} - \epsilon_{n_b}^j\|^2 + \sigma_{n_b} (\mathbf{V}_{n_b}^H \mathbf{V}_{n_b} - P_{n_b, \max}), \quad (30)$$

where σ_{n_b} is a Lagrange multiplier. Setting $\frac{\partial L_{\sigma}(\mathbf{V}_{n_b}, \epsilon_{n_b}^j)}{\partial \mathbf{V}_{n_b}} = 0$, we get the optimal solution as follows.

$$\mathbf{V}_{n_b}^{j+1}(\sigma_{n_b}) = \frac{1}{(1 + \sigma_{n_b})} \epsilon_{n_b}^j. \quad (31)$$

The optimal dual variable σ_{n_b} should satisfy the following complementary slackness condition.

$$\sigma_{n_b} (\mathbf{V}_{n_b}^H \mathbf{V}_{n_b} - P_{n_b, \max}) = 0. \quad (32)$$

If $\mathbf{V}_{n_b}^H \mathbf{V}_{n_b} < P_{n_b, \max}$, then $\sigma_{n_b} = 0$. Otherwise, we need to solve the equation $\mathbf{V}_{n_b}^H \mathbf{V}_{n_b} = P_{n_b, \max}$. By substituting (31) into the given equality, we derive the subsequent equation.

$$\frac{1}{(1 + \sigma_{n_b})^2} \|\epsilon_{n_b}^j\|^2 = P_{n_b, \max}. \quad (33)$$

Hence,

$$\sigma_{n_b} = \frac{\|\epsilon_{n_b}^j\|}{\sqrt{P_{n_b, \max}}} - 1. \quad (34)$$

Plugging (34) into (31), we get the optimal solution of \mathbf{V}_{n_b} .

$$\mathbf{V}_{n_b}^{j+1} = \frac{\sqrt{P_{n_b, \max}}}{\|\epsilon_{n_b}^j\|} \epsilon_{n_b}^j = \sqrt{P_{n_b, \max}} e^{j\vartheta(\epsilon_{n_b}^j)}. \quad (35)$$

where $\vartheta(\epsilon_{n_b}^j)$ denotes the phase angle of $\epsilon_{n_b}^j$. Therefore, we acquire $\mathbf{V}^{j+1} = [\mathbf{V}_1^{j+1}, \dots, \mathbf{V}_{N_b}^{j+1}]$ in (28) by parallel computation.

Remark 1: the precoding vector \mathbf{W} and the Lagrange multipliers $\boldsymbol{\sigma} = [\sigma_1, \dots, \sigma_{N_b}]^T$ were obtained using the primal-dual subgradient method (PDS) as described in [38]. In contrast to the PDS method, which involves iteratively solving a high-dimensional optimization problem for updating \mathbf{W} and $\boldsymbol{\sigma}$, our proposed approach is characterized by its simplicity and efficiency. This is because each subproblem in (24a) and (24b) has a closed-form solution that does not require iterative solving. Algorithm 1 summarizes the CADMM algorithm employed to solve the active precoding \mathbf{W} .

Algorithm 1 CADMM algorithm to solve the active precoding \mathbf{W}

- 1: Given (Φ, η) .
 - 2: **Repeat**
 - 3: Update δ by (17);
 - 4: Update \mathbf{W} by (27);
 - 5: Update \mathbf{V} by (35);
 - 6: Update \mathbf{q} by (24c);
 - 7: **Until** the problem $\mathcal{P}(2)$ converges.
-

D. Fix (η, \mathbf{W}) and solve Φ^{opt}

Given η and \mathbf{W} , we optimize Φ to address the $\mathcal{P}(1)$ problem in a more refined manner.

$$\mathcal{P}(4) : \max_{\Phi} f_4(\Phi) = \sum_{k=1}^K \sum_{m=1}^M \zeta_{k,m} f_{k,m}(\Phi, \mathbf{W}^*) \quad (36)$$

s.t. (9c), (9d).

Introduce a novel auxiliary function as

$$\mathbf{T}_{k,m,j}(\Phi_m) = \sum_{n_b=1}^{N_b} (\mathbf{H}_{n_b,k,m}^H + \mathbf{F}_{k,m}^H \Phi_m^H \mathbf{G}_{n_b,m}) \mathbf{w}_{n_b,m,j}. \quad (37)$$

f_4 can be rewritten as

$$f_4(\Phi) = \sum_{k=1}^K \sum_{m=1}^M \sqrt{\zeta_{k,m}} \mathbf{T}_{k,m,k}^H(\Phi_m) \left(\sum_{j=1}^K \mathbf{T}_{k,m,j}(\Phi_m) \mathbf{T}_{k,m,j}^H(\Phi_m) + \Xi_{k,m} \right)^{-1} \mathbf{T}_{k,m,k}(\Phi_m). \quad (38)$$

Let $\rho = [\rho_{1,1}, \rho_{1,2}, \dots, \rho_{1,K}, \rho_{2,1}, \rho_{2,2}, \dots, \rho_{M,K}]$, where $\rho_{m,k} \in \mathbb{C}^{N_r}$ is an auxiliary variable. Employing the MCQT in [64], the problem $\mathcal{P}(4)$ is reformulated as

$$\mathcal{P}(5): \max_{\Phi} f_5(\Phi, \rho) = \sum_{k=1}^K \sum_{m=1}^M g_{k,m}(\Phi_m, \rho) \quad (39)$$

s.t. (9c), (9d),

where

$$g_{k,m}(\Phi_m, \rho) = 2\sqrt{\zeta_{k,m}} \Re\{\rho_{k,m}^H \mathbf{T}_{k,m,k}(\Phi_m)\} - \rho_{k,m}^H \left(\sum_{j=1}^K \mathbf{T}_{k,m,j}(\Phi_m) \mathbf{T}_{k,m,j}^H(\Phi_m) + \Xi_{k,m} \right) \rho_{k,m}. \quad (40)$$

The variables ρ and Φ in the problem $\mathcal{P}(5)$ are updated alternatively. The update steps for the variables ρ and Φ are executed as follows.

D1. Fix Φ and Solve ρ^{opt}

The optimal value of ρ is obtained by fixing Φ in f_5 and setting $\partial f_5 / \partial \rho_{k,m} = 0$.

$$\rho_{k,m}^{\text{opt}} = \sqrt{\zeta_{k,m}} \left(\sum_{j=1}^K \mathbf{T}_{k,m,j}(\Phi_m) \mathbf{T}_{k,m,j}^H(\Phi_m) + \Xi_{k,m} \right)^{-1} \mathbf{T}_{k,m,k}(\Phi_m). \quad (41)$$

D2. Fix ρ and Solve Φ^{opt}

By substituting the optimal value ρ obtained in (41) into f_5 , it is observed that f_5 only depends on the variable Φ . Utilizing the function $\mathbf{T}_{k,m,j}(\Phi_m)$ from (38) and $\Phi_m = \text{diag}(\Phi_{1,m}, \dots, \Phi_{N_c,m})$, we can simplify the expression related to f_5 .

$$\begin{aligned} & \rho_{k,m}^H \mathbf{T}_{k,m,j}(\Phi_m) \\ &= \sum_{n_b=1}^{N_b} (\rho_{k,m}^H \mathbf{H}_{n_b,k,m}^H \mathbf{w}_{n_b,m,j} + \rho_{k,m}^H \mathbf{F}_{k,m}^H \Phi_m^H \mathbf{G}_{n_b,m} \mathbf{w}_{n_b,m,j}) \\ &= \sum_{n_b=1}^{N_b} \rho_{k,m}^H \mathbf{H}_{n_b,k,m}^H \mathbf{w}_{n_b,m,j} \\ &+ \phi_m^H \sum_{n_b=1}^{N_b} \text{diag}(\rho_{k,m}^H \mathbf{F}_{k,m}^H) \mathbf{G}_{n_b,m} \mathbf{w}_{n_b,m,j} \\ &= b_{k,m,j} + \phi_m^H \varpi_{k,m,j}, \end{aligned} \quad (42)$$

where

$$\phi_m = \Phi_m \mathbf{1}_{RN_c}, \quad (43a)$$

$$b_{k,m,j} = \sum_{n_b=1}^{N_b} \rho_{k,m}^H \mathbf{H}_{n_b,k,m}^H \mathbf{w}_{n_b,m,j}, \quad (43b)$$

$$\varpi_{k,m,j} = \sum_{n_b=1}^{N_b} \text{diag}(\rho_{k,m}^H \mathbf{F}_{k,m}^H) \mathbf{G}_{n_b,m} \mathbf{w}_{n_b,m,j}. \quad (43c)$$

Plugging (42) into (40), $g_{k,m}$ can be rewritten as

$$\begin{aligned} g_{k,m}(\phi_m) &= 2\sqrt{\zeta_{k,m}} \Re\{b_{k,m,k} + \phi_m^H \varpi_{k,m,k}\} \\ &- \sum_{j=1}^K (b_{k,m,j} + \phi_m^H \varpi_{k,m,j}) (b_{k,m,j}^* + \varpi_{k,m,j}^H \phi_m) \\ &- \rho_{k,m}^H \Xi_{k,m} \rho_{k,m}. \end{aligned} \quad (44)$$

Then f_5 in (39) can be refined in the following manner.

$$f_5(\phi_m) = \sum_{m=1}^M \left(-\phi_m^H \mathbf{Q}_m \phi_m + 2\Re\{\phi_m^H \mathbf{v}_m\} \right) - P, \quad (45)$$

where

$$\mathbf{Q}_m = \sum_{k=1}^K \sum_{j=1}^K \varpi_{k,m,j} \varpi_{k,m,j}^H, \quad (46a)$$

$$\mathbf{v}_m = \sum_{k=1}^K \sqrt{\zeta_{k,m}} \varpi_{k,m,k} - \sum_{k=1}^K \sum_{j=1}^K b_{k,m,j}^* \varpi_{k,m,j}, \quad (46b)$$

$$\begin{aligned} P &= \sum_{k=1}^K \sum_{m=1}^M \sum_{j=1}^K |b_{k,m,j}|^2 + \sum_{k=1}^K \sum_{m=1}^M \rho_{k,m}^H \Xi_{k,m} \rho_{k,m} \\ &- 2 \sum_{k=1}^K \sum_{m=1}^M \sqrt{\zeta_{k,m}} \Re\{b_{k,m,k}\}. \end{aligned} \quad (46c)$$

Define $\phi = [\phi_1^T, \phi_2^T, \dots, \phi_M^T]^T$, $\mathbf{v} = [\mathbf{v}_1^T, \mathbf{v}_2^T, \dots, \mathbf{v}_M^T]^T$, $\mathbf{Q} = \text{diag}(\mathbf{Q}_1, \mathbf{Q}_2, \dots, \mathbf{Q}_M)$,

Then f_5 in (45) can be rewritten in the compact manner.

$$f_5(\phi) = -\phi^H \mathbf{Q} \phi + 2\Re\{\phi^H \mathbf{v}\} - P, \quad (47)$$

Considering (4) and (9d), $\mathcal{P}(5)$ is equivalent to $\mathcal{P}(6)$:

$$\mathcal{P}(6): \min_{\phi, \varphi_{i,r}, \psi_{i,r}, \kappa_{i,r}} f_6(\phi) = \phi^H \mathbf{Q} \phi - 2\Re\{\phi^H \mathbf{v}\} \quad (48a)$$

$$\text{s.t. } \phi_{i,r,m} = \frac{\varphi_{i,r} f_m^2}{\psi_{i,r}^2 - f_m^2 + j\kappa_{i,r} f_m}, \quad (48a)$$

$$|\phi_{i,r,m}| \leq 1, \quad (48b)$$

$$\forall i \in \mathcal{N}_C, \forall r \in \mathcal{R}, \forall m \in \mathcal{M},$$

Due to the complex constraints in (48), problem $\mathcal{P}(6)$ is a difficult optimization problem, and its solution is a challenging task. To solve this issue, we employ the penalty-based approach, whereby the equality constraint (48a) is incorporated into the objective function as a penalty term. This results in the following optimization problem.

$$\mathcal{P}(7): \min_{\phi, \varphi, \psi, \kappa} f_7(\phi) = f_6(\phi) + \frac{1}{2\mu} \|\phi - \mathbf{b}(\varphi, \psi, \kappa)\|^2, \quad (48b)$$

s.t. (48b), $\forall i \in \mathcal{N}_C, \forall r \in \mathcal{R}, \forall m \in \mathcal{M}$.

The vector $\mathbf{b} \in \mathbb{C}^{MRN_c \times 1}$ corresponds to the equality constraint of (48a). $\varphi = [\varphi_{1,1}, \dots, \varphi_{1,R}, \dots, \varphi_{N_c,1}, \dots, \varphi_{N_c,R}]$, $\psi = [\psi_{1,1}, \dots, \psi_{1,R}, \dots, \psi_{N_c,1}, \dots, \psi_{N_c,R}]$, and $\kappa = [\kappa_{1,1}, \dots, \kappa_{1,R}, \dots, \kappa_{N_c,1}, \dots, \kappa_{N_c,R}]$. The parameter μ is employed to impose a penalty on the violation of the equality constraint (48a).

To address $\mathcal{P}(7)$, we propose an efficient algorithm based on APG and Fletcher-Reeves conjugate gradient method (FRCG) for solving the passive precoding problem, which will be discussed in the subsequent subsection.

D3. Fix φ, ψ, κ and solve ϕ

The APG method is employed to effectively tackle the optimization problem of ϕ through the iterative process outlined below.

$$\phi^{j+1} = \mathbf{y}^j - \frac{1}{\varpi^j} \nabla_{\phi} f_7(\mathbf{y}^j), \quad (49)$$

where \mathbf{y}^j is the extrapolated point.

$$\mathbf{y}^j = \phi^j + t_j (\phi^j - \phi^{j-1}), \quad (50)$$

with

$$t_j = \frac{d_j - 1}{d_j}, d_j = \frac{1 + \sqrt{1 + 4d_{j-1}^2}}{2}, d_0 = 0, \quad (51)$$

and ϖ^j is the step size¹. Let $\zeta^j = \mathbf{y}^j - \frac{1}{\varpi^j} \nabla_{\phi} f_7(\mathbf{y}^j)$, the projection can be obtained using the following formula.

$$\phi_{i,r,m}^{j+1} = \begin{cases} \frac{\zeta_{i,r,m}^j}{|\zeta_{i,r,m}^j|}, & |\zeta_{i,r,m}^j| > 1, \\ \zeta_{i,r,m}^j, & |\zeta_{i,r,m}^j| \leq 1, \\ e^{j\theta}, \theta \in [0, 2\pi], & \zeta_{i,r,m}^j = 0. \end{cases} \quad (52)$$

D4. Fix ϕ and solve φ, ψ, κ

After getting ϕ , solving φ, ψ, κ is equivalent to the following optimization.

$$\mathcal{P}(8) : \min_{\varphi, \psi, \kappa} f_8(\varphi, \psi, \kappa) = \|\phi - \mathbf{b}(\varphi, \psi, \kappa)\|^2,$$

This is an unconstrained optimization problem, which we solve using the FRCG algorithm. The iterations of this method consist of the following steps.

$$\begin{cases} \mathbf{z}^{j+1} = \mathbf{z}^j + \tau_j \mathbf{p}^j, \\ \mathbf{p}^{j+1} = -\nabla f_8(\mathbf{z}^j) + \lambda_j \mathbf{p}^j, \\ \lambda_j = \frac{\|\nabla f_8(\mathbf{z}^{j+1})\|^2}{\|\nabla f_8(\mathbf{z}^j)\|^2}, \\ \mathbf{p}^0 = -\nabla f_8(\mathbf{z}^0). \end{cases} \quad (53)$$

where \mathbf{z} represents one of φ, ψ, κ . τ_j is the step size.

Remark 2: The PDS method [38] was employed to solve passive precoding Φ in the narrowband systems, which involves iterative solutions for both Φ and Lagrangian multipliers $\chi = [\chi_1, \dots, \chi_{N_c R}]^{T2}$. Due to the large number of elements in the IRS, the complexity of the PDS method is significantly high. It is worth noting that the PDS method can not address the passive precoding Φ in the windband systems. In contrast, our proposed APG-FRCG algorithm offers

¹According to the Armijo rule, the step size utilized in [58] can be determined. However, this approach introduces an additional loop and increases the complexity of the algorithm. To address these limitations, we treat ϖ^j as a constant throughout the iterations.

²The symbol in [38] is utilized to represent the Lagrangian multipliers.

efficiency and simplicity as it provides closed-form solutions for Φ without requiring updates to Lagrangian multipliers χ . Algorithm 2 summarizes the APG-FRCG algorithm to solve passive precoding Φ .

Algorithm 2 APG-FRCG algorithm to solve $\mathcal{P}(4)$

-
- 1: Given (\mathbf{W}, η) . Set initial values for $\phi, \varphi, \psi, \kappa$, and tolerance $\varepsilon > 0$.
 - 2: **Repeat**
 - 3: Update ρ by (41);
 - 4: Update ϕ by (49)-(52);
 - 5: Update φ, ψ, κ by (53), respectively;
 - 6: **Until** the problem $\mathcal{P}(4)$ converges.
-

To date, we have addressed the joint precoding design for IRS-assisted cell-free networks. Based on the aforementioned discussion, we present Algorithm 3 as a summary of the CADMM-APG-FRCG algorithm to solve the problem of joint precoding design.

Algorithm 3 Joint precoding design algorithm based on the CADMM-APG-FRCG for $\mathcal{P}(1)$

-
- 1: **Initial** \mathbf{W}, Φ to a feasible solution.
 - 2: **Repeat**
 - 3: Update η by (15);
 - 4: Solve \mathbf{W} according to Algorithm 1;
 - 5: Solve Φ based on Algorithm 2;
 - 6: **Until** the problem $\mathcal{P}(1)$ converges.
-

E. Complexity analysis

The proposed CADMM-APG-FRCG algorithm for joint precoding design comprises three main components: updating variables η , solving active precoding \mathbf{W} and passive precoding Φ . The solution for \mathbf{W} involves updating $\delta, \mathbf{W}, \mathbf{V}$ and \mathbf{q} using (17), (27), (35) and (24c), respectively. Similarly, the solution for Φ requires updating $\rho, \phi, \varphi, \psi$, and κ using (41), (49)-(52) and (53), respectively. We evaluate the computational complexity (CC) of the CADMM-APG-FRCG algorithm in terms of complex multiplications (CMs). Since updating \mathbf{q} and \mathbf{V} do not need CMs, we only need to calculate CMs when updating $\eta, \delta, \mathbf{W}, \rho, \phi, \varphi, \psi$, and κ , respectively. The corresponding CM values are provided in Table. I, where I_W, I_ϕ and I_1 represent the iteration numbers for updating \mathbf{W}, ϕ and FRCG algorithm, respectively.

TABLE I: COMPUTATIONAL COMPLEXITIES

Variables	Computational complexities $\mathcal{O}(\cdot)$
η	$MK(KN_r N_t N_b + N_r^3 + (K+1)N_r^2 + N_r)$
δ	$MK(KN_r N_t N_b + N_r^3 + (K+1)N_r^2)$
\mathbf{W}	$N_t^2 N_b^2 M^2 K^2 + I_W N_t N_b M K$
ρ	$MK(N_r^3 + (K+1)N_r^2)$
ϕ	$I_\phi(N_c^2 R^2 + 2N_c R)$
φ	$3I_1 N_c R$
ψ	$3I_1 N_c R$
κ	$3I_1 N_c R$

Given the substantial number of BSs, users, and IRS elements in the IRS-assisted cell-free network, it is reasonable to

assume that $N_t N_b M K \gg N_r$ and $N_c R \gg N_r$ [9], [38], [39]. Based on this assumption and Table. I, it can be observed that the CCs of the overall algorithm depend primarily on those associated with the calculation of \mathbf{W} and Φ . Consequently, the CC of the overall algorithm can be expressed as $\mathcal{O}(I_{oC}(N_t^2 N_b^2 M^2 K^2 + I_W N_t N_b M K + I_\phi(N_c^2 R^2 + 2N_c R + 9I_1 N_c R)))$, where I_{oC} represents the number of iterations for the CADMM-APG-FRCG convergence.

IV. SIMULATION RESULTS

A. Simulation Configuration

In order to assess the performance of the CADMM-APG-FRCG algorithm in a cell-free network with IRS assistance, we conducted simulations under various conditions. We followed the deployment scheme used in previous studies [4], [38] (see Fig. 5 in [38]), where four users were simultaneously served by five BSs. To address capacity limitations caused by obstructions in green areas, we placed two IRSs independently on different building surfaces. For our simulation setup, we considered a three-dimensional coordinate system. The j -th BS was positioned at coordinates $(40(j-1)\text{m}, -50\text{m}, 3\text{m})$, while the IRSs were located at coordinates $(30\text{m}, 10\text{m}, 6\text{m})$ and $(130\text{m}, 10\text{m}, 6\text{m})$. We incorporated a distance-dependent path loss model to account for propagation loss.

$$L(\tilde{d}) = c_0 \left(\frac{\tilde{d}}{d_0} \right)^{-\zeta}, \quad \tilde{d} \in \{\tilde{d}_{BU}, \tilde{d}_{IU}, \tilde{d}_{BI}\}, \zeta \in \{\zeta_{BU}, \zeta_{IU}, \zeta_{BI}\} \quad (54)$$

where $c_0 = -30\text{dB}$ represents the path loss at the reference distance $d_0 = 1\text{ m}$, ζ denotes the path loss exponent, and \tilde{d} indicates the link distance. The link distances between the BS and user, IRS and user, BS and IRS are denoted by \tilde{d}_{BU} , \tilde{d}_{IU} , and \tilde{d}_{BI} , respectively. ζ_{BU} , ζ_{IU} , and ζ_{BI} are corresponding path loss exponent of them, respectively. In the following simulations, we take $\zeta_{BU} = 3.5$, $\zeta_{IU} = 2.8$, and $\zeta_{BI} = 2.2$. In this cell-free network scenario, each BS is equipped with a limited number of antennas and operates at low transmit power. Therefore, we set the maximum transmit power of each BS as $P_{n_b, max} = 0\text{ dBm}$. The number of antennas per BS is $N_t = 2$, while each user has $N_r = 2$ antennas. Additionally, there are $R = 100$ units per IRS and $M = 16$ tones in use. The Lorentzian parameters were initialized as: $\varphi_{i,r} = 1$, $\psi_{i,r} = 3 \times 10^9$, $Q_n = 50$, $\kappa_{i,r} = \frac{\psi_{i,r}}{Q_n} = 6 \times 10^7$, $f_c = 3\text{ GHz}$ and $B = 100\text{ MHz}$. The noise power τ^2 is assumed to be -80 dBm [25]. We adopt the Rice fading channel model for our analysis.

$$\mathbf{H} = \sqrt{\frac{\varepsilon}{1+\varepsilon}} \mathbf{H}_{LoS} + \sqrt{\frac{1}{1+\varepsilon}} \mathbf{H}_{NLoS}, \quad (55)$$

$$\mathbf{H} \in \{\mathbf{H}_{BU}, \mathbf{H}_{IU}, \mathbf{H}_{BI}\}; \varepsilon \in \{\varepsilon_{BU}, \varepsilon_{IU}, \varepsilon_{BI}\},$$

where ε denotes the Rice factor. \mathbf{H}_{LoS} and \mathbf{H}_{NLoS} stand for the line-of-sight (LoS) and Rayleigh fading component, respectively. When $\varepsilon \rightarrow \infty$, \mathbf{H} corresponds to a LoS channel. As $\varepsilon \rightarrow 0$, \mathbf{H} is a Rayleigh fading channel. In addition, we assume $\varepsilon_{BU} \rightarrow 0$, $\varepsilon_{BI} \rightarrow \infty$ and $\varepsilon_{IU} \rightarrow 0$ in simulations. The

weight factor is assumed to be $\xi_{k,m} = 1$. In the CADMM-APG-FRCG algorithm, we select the parameters $\alpha = N_b$, $\beta = \frac{\mathbf{W}^H \mathbf{D} \mathbf{W}}{\mathbf{W}^H \mathbf{W}}$, $\varpi = \frac{1}{8}$, and $\mu = 12 \frac{N_b^2}{\phi^H \mathbf{Q} \phi}$.

We also assume that the users are uniformly distributed within a circular area with a radius of 10 m, centered at $(L, 0)$, and that all users have a height of 1.5 m. To evaluate the performance of the proposed CADMM-APG-FRCG algorithm compared to the PDS method [38] in an IRS-assisted cell-free system, we consider four baselines.

Optimized phase shift: Maximizing the WSR is achieved through Algorithm. 3.

Without direct link: Maximizing the WSR is achieved via Algorithm. 3, where direct links between BSs and users are obstructed, leaving only indirect channels available.

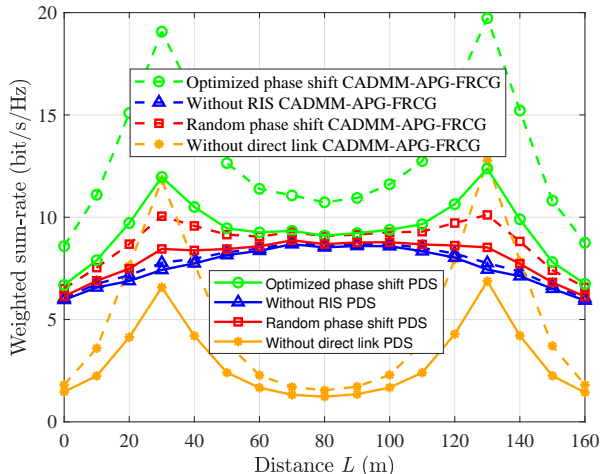
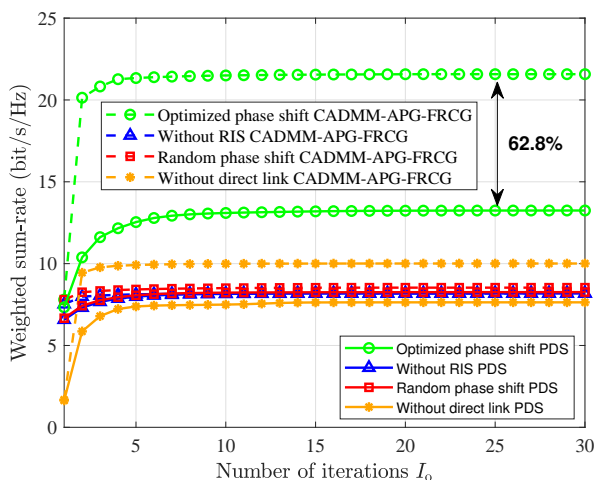
Random phase shift: Maximizing the WSR only at BSs based on Algorithm. 3 by randomly setting the phase shift of all IRS reflection units.

Without IRS: By utilizing the CSI between BSs and users, the optimization of WSR is executed through a precoding method implemented at the BSs.

B. Performance of the Proposed CADMM-APG-FRCG Algorithm

Fig. 2 illustrates that both the PDS and CADMM-APG-FRCG algorithms exhibit two peaks of the WSR at $L = 30$ and $L = 130$, except for scenarios without IRS or with random phase shift. This observation suggests that the WSR improves as users approach IRSs. Nevertheless, when a random phase shift is considered for the wideband case, there is only a modest increase in WSR in comparison to scenarios without IRS. In contrast, the narrowband case exhibits minimal variation. These findings indicate that proper optimization of passive beamforming can significantly enhance WSR in cell-free networks through the use of IRS. Moreover, it is noteworthy that, with the exception of the cases without IRS and with random phase shift, across all scenarios considered, the CADMM-APG-FRCG algorithm consistently outperforms the PDS algorithm, demonstrating a more substantial improvement in WSR performance. This validates the effectiveness of the CADMM-APG-FRCG algorithm in maximizing WSR in the presence of IRS.

Fig. 3 demonstrates the convergence of the CADMM-APG-FRCG algorithm and the PDS method in a cell-free system with IRS assistance. The horizontal axis represents the number of iterations. When setting $L = 30$ and keeping other parameters constant, it is evident that across three scenarios, namely the ideal case, the continuous phase shift case and the case without a direct link, the CADMM-APG-FRCG algorithm consistently outperforms the PDS method in terms of WSR values. From Fig. 3, we can see that the PDS algorithm requires 15 iterations to converge, whereas the CADMM-APG-FRCG algorithm requires only 10 iterations to achieve convergence. As the CADMM-APG-FRCG algorithm necessitates a lesser number of iterations than the PDS algorithm, its complexity is considerably lower than that of the PDS algorithm, as illustrated in Table. II below. This markedly reduces the time required for simulations to address problem

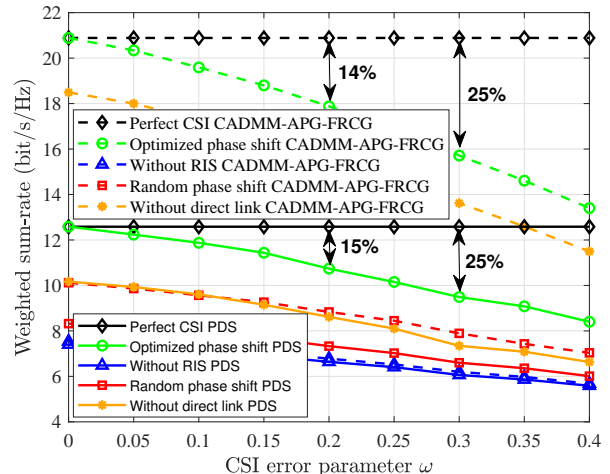
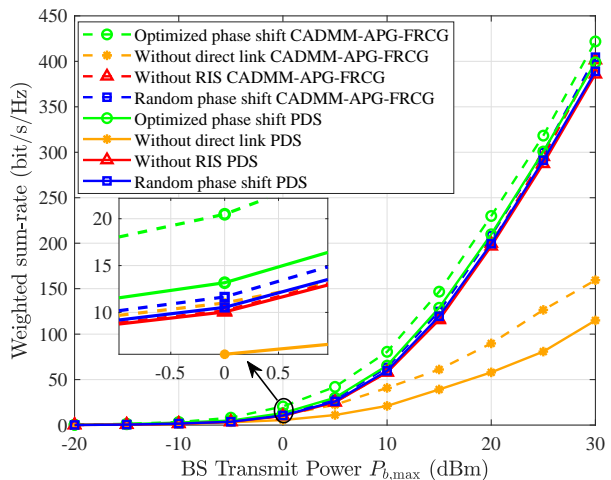
Fig. 2: Weighted sum-rate against the distance L .Fig. 3: Weighted sum-rate against the number of iterations I_0 .

$\mathcal{P}(0)$, thereby rendering our CADMM-APG-FRCG algorithm a viable option for engineering applications. Furthermore, it is evident that upon convergence, the WSR obtained by the CADMM-APG-FRCG algorithm is approximately 62.8% greater than that of the PDS algorithm. This indicates that the PDS algorithm only attains a suboptimal solution. The underlying reason for this is that the CADMM-APG-FRCG algorithm optimally solves \mathbf{W} and Φ in $\mathcal{P}(0)$.

It is challenging to obtain accurate CSI in IRS-assisted cell-free networks, even with the assumption of perfect CSI. In Fig. 4, we investigate the relationship between the WSR and the error in channel estimation. We model the actual estimated channel as follows [38].

$$\tilde{\mathbf{H}} = \mathbf{H} + \Delta\mathbf{H}, \quad (56)$$

The practical channel is represented by \mathbf{H} , and the estimation error is denoted as $\Delta\mathbf{H}$, where $\Delta\mathbf{H} \sim \mathcal{CN}(0, \tau_H^2 \mathbf{I})$. To characterize the CSI estimation error, we assume $\tau_H^2 = \omega \|\mathbf{H}\|^2$. As illustrated in Fig. 4, the degradation of WSR performance is evident as the error ω increases. In comparison

Fig. 4: Weighted sum-rate against the CSI error parameter ω .Fig. 5: Weighted sum-rate against the BS transmit power $P_{b,\max}$.

to the scenario of perfect CSI ($\omega = 0$), when $\omega = 0.2$, the PDS algorithm exhibits a WSR performance loss of approximately 15%, while CADMM-APG-FRCG shows a loss of about 14%. With $\omega = 0.3$, the WSR performance loss for the PDS algorithm and CADMM-APG-FRCG reaches about 25% and 25%, respectively. It can be observed that both algorithms exhibit similar resilience to CSI estimation errors. However, it is worth noting that the WSR obtained by the CADMM-APG-FRCG algorithm is 66.6% and 65.7% higher than that of the PDS algorithm when $\omega = 0.2$ and $\omega = 0.3$, respectively.

To examine the influence of various system parameters on system performance, we relocated four users to positions $(20m, 0)$, $(60m, 0)$, $(100m, 0)$, $(140m, 0)$. Fig. 5 depicts the relationship between the average WSR and the BS transmission power. It can be observed that an increase in the BS transmit power results in an elevated average WSR. Intuitively, the similarity between the CADMM-APG-FRCG and PDS algorithms lies in the fact that when the BS transmission power is insufficient, the signal reflected by the RIS is very weak and does not significantly contribute to performance improvement. Conversely, when the BS transmission power

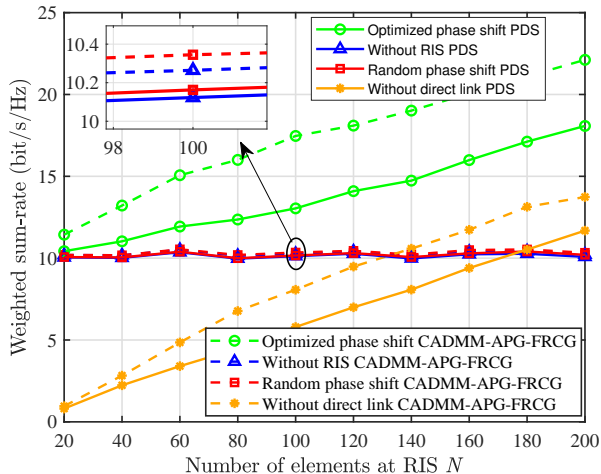


Fig. 6: Weighted sum-rate against the number of RIS elements.

is excessive, the BS tends to allocate most of the power to the beam aimed at the BS-user link rather than the BS-RIS-user link, making the role of RISs less significant. This explains the difference between the "Without RIS" and "Without direct link" scenarios, and as the BS transmission power increases, the gap between the two methods becomes more pronounced. Therefore, a better selection of BS transmission power is crucial to fully leverage the use of RIS in RIS-aided cell-free networks. However, it is noteworthy that among all the aforementioned schemes, the PDS method yields suboptimal solutions, whereas the CADMM-APG-FRCG method achieves optimal solutions. Consequently, the CADMM-APG-FRCG algorithm outperforms the PDS algorithm in terms of WSR performance, when the BS transmission power is large or equal to 0 dBm.

The relationship between the number of IRS units and the WSR is illustrated in Fig. 6, using the same settings as Fig. 5. As can be observed in Fig. 6, the average WSR of IRS-assisted cell-free systems increases with an increase in the number of IRS units in all three cases, namely, the ideal case, continuous phase shift case and without direct link case. In cases involving random phase shift and without IRS, the incorporation of additional IRS units exerts a negligible influence on the WSR performance, as observed in both the PDS and CADMM-APG-FRCG methods. However, for the two methods, random phase shift results in a slightly superior WSR in comparison to the case without IRS. It should be noted that since ϕ has a dimension of MRN_c , the calculation of the WSR becomes more complex with an increasing number of IRS units. This, in turn, presents a challenge in channel estimation. Therefore, it is necessary to strike a balance between achieving optimal WSR performance and determining an appropriate number of IRS units to use. Furthermore, it has been observed that the CADMM-APG-FRCG algorithm significantly outperforms the PDS algorithm in terms of the WSR obtained.

The computational complexity between the CADMM-APG-

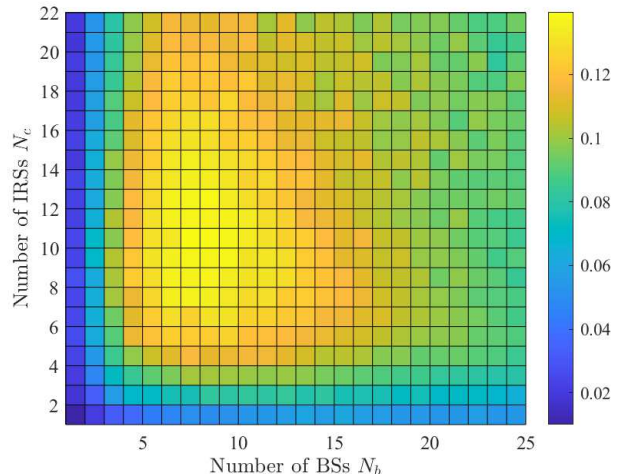


Fig. 7: Energy efficiency of the system in CADMM-APG-FRCG method against BS number N_b and IRS number N_c .

FRCG and PDS algorithms is compared in Table II³. To illustrate the low CC property of the CADMM-APG-FRCG, we provide the computational complexity ratio (CCR) of the CADMM-APG-FRCG algorithm versus the PDS one. The CCR is defined as follows.

$$\text{CCR} = \frac{\text{the overall CC of CADMM-APG-FRCG}}{\text{the overall CC of PDS}}. \quad (57)$$

The $\text{CCR} = \frac{2.408E+7}{7.6584E+7} = 31.4426\%$, which indicates a 68.5574% lower CC compared to that of the PDS. Based on Fig. 2-Fig. 6 and Table. II, it can be observed that the CADMM-APG-FRCG algorithm exhibits superior WSR performance and lower computational complexity when solving the problem $\mathcal{P}(1)$ compared to the PDS algorithm. Therefore, the proposed CADMM-APG-FRCG method presents itself as a highly promising approach for addressing complex optimization problems $\mathcal{P}(1)$.

In Fig. 7, we investigate the correlation between the energy efficiency of the CADMM-APG-FRCG algorithm and the number of BS and IRS, with the aim of improving the capacity of the system through the use of IRS with low power consumption and cost-effectiveness. The energy efficiency of the system is quantified using a formula derived from references [22] and [38].

$$E_{ee} = \frac{R_{sum}}{\hat{\lambda} \|\mathbf{W}\| + N_b P_B + K P_U + N_c R P_I}, \quad (58)$$

where $\hat{\lambda}^{-1}$ denotes the efficiency of the transmit power amplifier, and P_B , P_U , and P_I represents the power consumption at each BS, each user and each IRS unit, respectively. We adopt the same configuration as the reference [38], that is, $\lambda = 1.2$, $P_B = 9$ dBW, $P_U = 10$ dBm, $P_I = 10$ dBm, $M = N_t = N_r = 1$ and $R = 20$, with the corresponding distances set to $d_{BU} = d_{BI} = 110$ m and $d_{IU} = 15$ m. As illustrated in Fig. 7, the energy efficiency does not increase

³For the complexity of the PDS method, we use the symbol in [38]. Here, I_{oCA} , I_W , I_ϕ , I_1 , I_o , I_a and I_p are based on the average of 100 channel experiments.

TABLE II: Computational complexity comparison between the CADMM-APG and PDS algorithms

Methods	CC $\mathcal{O}(\cdot)$	Number of iterations	Overall CC
CADMM-APG-FRCG	$\mathcal{O}(I_{oC}(N_t^2 N_b^2 M^2 K^2 + I_W N_t N_b M K + I_\phi(N_c^2 R^2 + 2N_c R + 9I_1 N_c R)))$	$I_{oC} = 10, I_W = 35, I_\phi = 40, I_1 = 5$	2.408E+7
PDS	$\mathcal{O}(I_o(I_a N_t^2 N_b^2 M^2 K^2 + I_p N_c^2 R^2))$	$I_o = 15, I_a = 11, I_p = 15$	7.6584E+7
	CCR		31.4426%

monotonically with the growth of N_b and N_c . When N_b is held constant, an initial enhancement in energy efficiency is followed by a subsequent decrease as N_c increases. When $N_b = 7$ and $N_c = 10$, E_{ee} reaches its maximum value at this point with a value of 0.1394 bit/s/Hz/W being achieved. However, when $N_b = 7$ and $N_c = 22$, E_{ee} drops to 0.1129 bit/s/Hz/W, resulting in a decrease of approximately 19.01% in energy efficiency. In comparison to the PDS method⁴, the CADMM-APG-FRCG algorithm demonstrates a more gradual decline in energy efficiency than the PDS algorithm. This offers a broader range of possibilities for the selection of energy efficiency and the number of BSs and IRSs in a practical system.

V. CONCLUSION

This paper investigates the use of IRS-assisted cell-free networks in a wideband scenario to enhance network capacity while minimizing costs and power consumption. The aim is to maximize the system's WSR by jointly optimizing the precoding design, considering power constraints at BSs and phase shift constraints at the IRSs. To solve this non-convex optimization problem, the paper employs the Lagrangian dual transform to decouple the problem and utilizes fractional programming to address the active and passive beamforming optimizations. Specifically, the CADMM-APG-FRCG algorithm is proposed to solve the corresponding subproblems. Simulation results demonstrate that the CADMM-APG-FRCG scheme outperforms the primal-dual subgradient (PDS) method in terms of WSR performance while maintaining a lower complexity. This indicates that the CADMM-APG-FRCG algorithm offers significant advantages for optimizing network capacity in IRS-assisted cell-free networks.

REFERENCES

- [1] M. Kamel, W. Hamouda, and A. Youssef, "Ultra-dense networks: A survey," *IEEE Commun. Surveys Tuts.*, vol. 18, no. 4, pp. 2522-2545, Oct.-Dec. 2016.
- [2] R. Borralho, A. Mohamed, A. U. Quddus, P. Vieira and R. Tafazolli, "A survey on coverage enhancement in cellular networks: challenges and solutions for future deployments," *IEEE Commun. Surveys Tuts.*, vol. 23, no. 2, pp. 1302-1341, Secondquarter 2021.
- [3] E. Nayebi, A. Ashikhmin, T. L. Marzetta, and H. Yang, "Cell-free massive MIMO systems," in *Proc. 49th Asilomar Conf. Signals Syst. Comput.*, 2015, pp. 695-699.
- [4] G. Interdonato, E. Björnson, H. Q. Ngo, P. Frenger, and E. G. Larsson, "Ubiquitous cell-free massive MIMO communications," *EURASIPJ. Wireless Commun. Netw.*, pp. 197-206, 2019.
- [5] S. Mosleh, H. Almosa, E. Perrins, and L. Liu, "Downlink resource allocation in cell-free massive MIMO systems," in *Proc. Int. Conf. Comput. Netw. Commun.*, 2019, pp. 883-887.

⁴The maximum energy efficiency of the PDS method is 0.138 bit/s/Hz/W in [38], the corresponding decrease in energy efficiency is 34.7%.

- [6] M. Attarifar, A. Abbasfar, and A. Lozano, "Modified conjugate beamforming for cell-free massive MIMO," *IEEE Commun. Lett.*, vol. 8, no. 2, pp. 616-619, Apr. 2019.
- [7] Y. Jin, J. Zhang, S. Jin, and B. Ai, "Channel estimation for cell-free mmwave massive MIMO through deep learning," *IEEE Trans. Veh. Technol.*, vol. 68, no. 10, pp. 10325-10329, Oct. 2019.
- [8] J. G. Andrews, X. Zhang, G. D. Durgin, and A. K. Gupta, "Are we approaching the fundamental limits of wireless network densification?," *IEEE Commun. Mag.*, vol. 54, no. 10, pp. 1558-1896, Oct. 2016.
- [9] H. Q. Ngo, A. Ashikhmin, H. Yang, E. G. Larsson, and T. L. Marzetta, "Cell-free massive MIMO versus small cells," *IEEE Trans. Wireless Commun.*, vol. 16, no. 3, pp. 1834-1850, Mar. 2017.
- [10] Q. Wu and R. Zhang, "Towards smart and reconfigurable environment: Intelligent reflecting surface aided wireless network," *IEEE Commun. Mag.*, vol. 58, no. 1, pp. 106-112, Jan. 2020
- [11] Q. Wu, S. Zhang, B. Zheng, C. You and R. Zhang, "Intelligent reflecting surface-aided wireless communications: a tutorial," *IEEE Trans. Commun.*, vol. 69, no. 5, pp. 3313-3351, May 2021.
- [12] L. Dai, *et al.*, "Reconfigurable intelligent surface-based wireless communication: Antenna design, prototyping and experimental results," *IEEE Access.*, vol. 8, pp. 45913-45923, Mar. 2020.
- [13] Q. Wu, X. Zhou, W. Chen, J. Li and X. Zhang, "IRS-aided WPCNs: a new optimization framework for dynamic IRS beamforming," *IEEE Trans. Wireless Commun.*, vol. 21, no. 7, pp. 4725-4739, July. 2022.
- [14] G. Chen, Q. Wu, R. Liu, J. Wu and C. Fang, "IRS aided MEC systems with binary offloading: a unified framework for dynamic IRS beamforming," *IEEE J. Sel. Areas Commun.*, vol. 41, no. 2, pp. 349-365, Feb. 2023.
- [15] Z. Sun and Y. Jing, "On the performance of multi-antenna IRS-assisted NOMA networks with continuous and discrete IRS phase shifting," *IEEE Trans. Wireless Commun.*, vol. 21, no. 5, pp. 3012-3023, May. 2022.
- [16] C. Liaskos, *et al.*, "A new wireless communication paradigm through software-controlled metasurfaces," *IEEE Commun. Mag.*, vol. 56, no. 9, pp. 162-169, Sep. 2018.
- [17] Z. Li, W. Chen, Q. Wu, K. Wang and J. Li, "Joint beamforming design and power splitting optimization in IRS-assisted SWIPT NOMA networks," *IEEE Trans. Wireless Commun.*, vol. 21, no. 3, pp. 2019-2033, Mar. 2022.
- [18] M. Di Renzo *et al.*, "Smart radio environments empowered by reconfigurable AI meta-surfaces: An idea whose time has come," *EURASIPJ. Wireless Commun. Netw.*, vol. 2019, no. 1, pp. 129, 2019.
- [19] Y. Li, H. Zhang, K. Long and A. Nallanathan, "Exploring sum rate maximization in UAV-based multi-IRS networks: IRS association, UAV altitude, and phase shift design," *IEEE Trans. Commun.*, vol. 70, no. 11, pp. 7764-7774, Nov. 2022.
- [20] K. Ntontin, *et al.*, "Reconfigurable intelligent surfaces vs. relaying: differences, similarities, and performance comparison," *IEEE Open Access J. Commun. Soc.*, vol. 1, pp. 798-807, 2020.
- [21] S. Wang, Q. Li and M. Shao, "One-bit symbol-level precoding for MU-MISO downlink with intelligent reflecting surface," *IEEE Signal Process. Lett.*, vol. 27, pp. 1784-1788, 2020.
- [22] C. Huang, A. Zappone, G. C. Alexandropoulos, M. Debbah and C. Yuen, "Reconfigurable intelligent surfaces for energy efficiency in wireless communication," *IEEE Trans. Wireless Commun.*, vol. 18, no. 8, pp. 4157-4170, Aug. 2019.
- [23] Y. Lin, S. Jin, M. Matthaiou and X. You, "Channel estimation and user localization for IRS-assisted MIMO-OFDM systems," *IEEE Trans. Wireless Commun.*, vol. 21, no. 4, pp. 2320-2335, Apr. 2022.
- [24] Y. Lin, S. Jin, M. Matthaiou and X. You, "Conformal IRS-empowered MIMO-OFDM: channel estimation and environment mapping," *IEEE Trans. Commun.*, vol. 70, no. 7, pp. 4884-4899, Jul. 2022.
- [25] Q. Wu and R. Zhang, "Intelligent reflecting surface enhanced wireless network via joint active and passive beamforming," *IEEE Trans. Wireless Commun.*, vol. 18, no. 11, pp. 5394-5409, Nov. 2019.
- [26] Y. He, Y. Cai, H. Mao and G. Yu, "RIS-assisted communication radar coexistence: joint beamforming design and analysis," *IEEE J. Sel. Areas Commun.*, vol. 40, no. 7, pp. 2131-2145, 2022.

- [27] Q.-U.-A. Nadeem, A. Kammoun, A. Chaaban, M. Debbah and M.-S. Alouini, "Asymptotic max-min SINR analysis of reconfigurable intelligent surface assisted MISO systems," *IEEE Trans. Commun.*, vol. 19, no. 12, pp. 7748-7764, Dec. 2020.
- [28] M. Najafi, V. Jamali, R. Schober and H. V. Poor, "Physics-based modeling and scalable optimization of large intelligent reflecting surfaces," *IEEE Trans. Commun.*, vol. 69, no. 4, pp. 2673-2691, Apr. 2021.
- [29] C. Pan, *et al.*, "Multicell MIMO communications relying on intelligent reflecting surfaces," *IEEE Trans. Wireless Commun.*, vol. 19, no. 8, pp. 5218-5233, Aug. 2020.
- [30] S. Abeywickrama, R. Zhang, Q. Wu and C. Yuen, "Intelligent reflecting surface: practical phase shift model and beamforming optimization," *IEEE Trans. Commun.*, vol. 68, no. 9, pp. 5849-5863, Sep. 2020.
- [31] W. Yan, X. Yuan, Z. -Q. He and X. Kuai, "Passive beamforming and information transfer design for reconfigurable intelligent surfaces aided multiuser MIMO systems," *IEEE J. Sel. Areas Commun.*, vol. 38, no. 8, pp. 1793-1808, Aug. 2020.
- [32] V. Kumar, M. F. Flanagan, R. Zhang and L. -N. Tran, "Achievable rate maximization for underlay spectrum sharing MIMO system with intelligent reflecting surface," *IEEE Wireless Commun. Lett.*, vol. 11, no. 8, pp. 1758-1762, Aug. 2022.
- [33] L. You, *et al.*, "Energy efficiency and spectral efficiency tradeoff in RIS-aided multiuser MIMO uplink transmission," *IEEE Trans. Signal Process.*, vol. 69, pp. 1407-1421, 2021.
- [34] Y. Su, X. Pang, S. Chen, X. Jiang, N. Zhao and F. R. Yu, "Spectrum and energy efficiency optimization in IRS-assisted UAV networks," *IEEE Trans. Commun.*, vol. 70, no. 10, pp. 6489-6502, Oct. 2022.
- [35] X. Pang, N. Zhao, J. Tang, C. Wu, D. Niyato and K. -K. Wong, "IRS-assisted secure UAV transmission via joint trajectory and beamforming design," *IEEE Trans. Commun.*, vol. 70, no. 2, pp. 1140-1152, Feb. 2022.
- [36] H. Xie, J. Xu and Y. -F. Liu, "Max-Min fairness in IRS-aided multi-cell MISO systems with joint transmit and reflective beamforming," *IEEE Trans. Wireless Commun.*, vol. 20, no. 2, pp. 1379-1393, Feb. 2021.
- [37] Q. -U. -A. Nadeem, A. Zappone and A. Chaaban, "Achievable rate analysis and Max-Min SINR optimization in intelligent reflecting surface assisted cell-free MIMO uplink," *IEEE Open Access J. Commun. Soc.*, vol. 3, pp. 1295-1322, 2022.
- [38] Z. Zhang and L. Dai, "A joint precoding framework for wideband reconfigurable intelligent surface-aided cell-free network," *IEEE Trans. Signal Process.*, vol. 69, pp. 4085-4101, 2021.
- [39] P. Wang, J. Fang, X. Yuan, Z. Chen, and H. Li, "Intelligent reflecting surface-assisted millimeter wave communications: joint active and passive precoding design," *IEEE Trans. Veh. Technol.*, vol. 69, no. 12, pp. 14960-14973, Dec. 2020.
- [40] B. Di, *et al.*, "Hybrid beamforming for reconfigurable intelligent surface based multi-user communications: achievable rates with limited discrete phase shifts," *IEEE J. Sel. Areas Commun.*, vol. 38, no. 8, pp. 1809-1822, Aug. 2020.
- [41] Y. Yang, S. Zhang, and R. Zhang, "IRS-enhanced OFDM: power allocation and passive array optimization," in *Proc. IEEE Global Commun. Conf.*, 2019, pp. 1-6.
- [42] M. Hua, Q. Wu, C. He, S. Ma, and W. Chen, "Joint active and passive beamforming design for IRS-aided radar-communication," *IEEE Trans. Wireless Commun.*, vol. 22, no. 4, pp. 2278-2294, Apr. 2023.
- [43] Q. Peng, Q. Wu, G. Chen, R. Liu, S. Ma, and W. Chen, "Hybrid active-passive IRS assisted energy-efficient wireless communication," *IEEE Commun. Lett.*, vol. 27, no. 8, pp. 2202-2206, Aug. 2023.
- [44] Y. Han, S. Zhang, L. Duan, and R. Zhang, "Cooperative double-IRS aided communication: beamforming design and power scaling," *IEEE Wireless Commun. Lett.*, vol. 9, no. 8, pp. 1206-1210, Aug. 2020.
- [45] B. Zheng, C. You, and R. Zhang, "Double-IRS assisted multi-user MIMO: cooperative passive beamforming design," *IEEE Trans. Wireless Commun.*, vol. 20, no. 7, pp. 4513-4526, Jul. 2021.
- [46] E. Dong, Z. Lian, Y. Wang, Z. Ma, L. Ling and C. Luo, "Double-IRS Auxiliary Communications: Models and Performance Prediction," *IEEE Wireless Commun. Lett.*, vol. 13, no. 9, pp. 2571-2575, Sep. 2024.
- [47] E. Shi *et al.*, "RIS-aided cell-free massive MIMO systems for 6G: fundamentals, system design, and applications," *Proc. IEEE.*, vol. 112, no. 4, pp. 331-364, Apr. 2024.
- [48] X. Qiao, Y. Zhang, J. Zhang, H. Fang, L. Yang and H. Zhu, "Novel beamforming design for IRS-assisted cell-free massive MIMO systems," *IEEE Wireless Commun. Lett.*, vol. 13, no. 4, pp. 1068-1072, Apr. 2024.
- [49] C. Chen, S. Xu, J. Zhang and J. Zhang, "A distributed machine learning-based approach for IRS-enhanced cell-free MIMO networks," *IEEE Trans. Wireless Commun.*, vol. 23, no. 5, pp. 5287-5298, May. 2024.
- [50] Y. Zhang, H. Zhao, W. Xia, L. Yang and H. Zhu, "Rate analysis and optimization of IRS-aided hardware-impaired cell-free massive MIMO systems under correlated Rician fading channels," *IEEE Trans. Veh. Technol.*, vol. 73, no. 8, pp. 12126-12131, Aug. 2024.
- [51] H. Li *et al.*, "Intelligent reflecting surface enhanced wideband MIMO-OFDM communications: From practical model to reflection optimization," *IEEE Trans. Commun.*, vol. 69, no. 7, pp. 4807-4820, Jul. 2021.
- [52] G. Lee, H. Lee, D. Kim, J. Chung, A. L. Swindlehurst and J. Choi, "Joint downlink and uplink optimization for RIS-aided FDD MIMO communication systems," *IEEE Trans. Wireless Commun.*, vol. 23, no. 8, pp. 9059-9071, Aug. 2024.
- [53] L. Pulido-Mancera *et al.*, "Polarizability extraction of complementary metamaterial elements in waveguides for aperture modeling," *Phys. Rev. B.*, vol. 96, no. 23, p. 235402, 2017.
- [54] N. Shlezinger *et al.*, "Dynamic metasurface antennas for 6G extreme massive MIMO communications," *IEEE Wireless Commun.*, vol. 28, no. 2, pp. 106-113, Jan. 2021.
- [55] H. Wang *et al.*, "Dynamic metasurface antennas for MIMO-OFDM receivers with bit-limited ADCs," *IEEE Trans. Commun.*, vol. 69, no. 4, pp. 2643-2659, Apr. 2021.
- [56] N. Shlezinger *et al.*, "Dynamic metasurface antennas for uplink massive MIMO systems," *IEEE Trans. Commun.*, vol. 67, no. 10, pp. 6829-6843, Oct. 2019.
- [57] K. D. Katsanos¹, N. Shlezinger, M. F. Imani, and G. C. Alexandropoulos, "Wideband multi-user MIMO communications with frequency selective RISs: element response modeling and sum-rate maximization," *arXiv:2202.02169v2 [cs.IT] 25 Mar 2022*.
- [58] H. Guo, Y. -C. Liang, J. Chen, *et al.*, "Weighted sum-rate maximization for reconfigurable intelligent surface aided wireless networks," *IEEE Trans. Wireless Commun.*, vol. 19, no. 5, pp. 3064-3076, May. 2020.
- [59] H. Guo, Y. -C. Liang, J. Chen, *et al.*, "Weighted sum-rate optimization for intelligent reflecting surface enhanced wireless networks," in *Proc. IEEE Global Commun. Conf.*, Waikoloa, HI, USA, 2019, pp. 1-6.
- [60] W. Du, *et al.*, "Weighted sum-rate and energy efficiency maximization for joint ITS and IRS assisted multiuser MIMO networks," *IEEE Trans. Commun.*, vol. 70, no. 11, pp. 7351-7364, Nov. 2022.
- [61] P. Zeng, D. Qiao, H. Qian and Q. Wu, "Joint beamforming design for IRS aided multiuser MIMO with imperfect CSI," *IEEE Trans. Veh. Technol.*, vol. 71, no. 10, pp. 10729-10743, Oct. 2022.
- [62] Q. Tao, S. Zhang, C. Zhong, W. Xu, H. Lin and Z. Zhang, "Weighted sum-rate of intelligent reflecting surface aided multiuser downlink transmission with statistical CSI," *IEEE Trans. Wireless Commun.*, vol. 21, no. 7, pp. 4925-4937, Jul. 2022.
- [63] Y. Wang, L. Fang, S. Cai, Z. Lian, Y. Su, and Z. Xie, "Low-complexity algorithm for maximizing the weighted sum-rate of intelligent reflecting surface assisted wireless networks," *IEEE Internet Things J.*, vol. 11, no. 6, pp. 10490-10499, Mar. 2024.
- [64] K. Shen and W. Yu, "Fractional programming for communication systems Part I: Power control and beamforming," *IEEE Trans. Signal Process.*, vol. 66, no. 10, pp. 2616-2630, May. 2018.
- [65] K. Shen and W. Yu, "Fractional programming for communication systems," Part II: Uplink scheduling via matching," *IEEE Trans. Signal Process.*, vol. 66, no. 10, pp. 2631-2644, 2018.
- [66] K. Huang and N. D. Sidiropoulos, "Consensus-ADMM for General Quadratically Constrained Quadratic Programming," *IEEE Trans. Signal Process.*, vol. 64, no. 20, pp. 5297-5310, 15 Oct. 15, 2016.
- [67] H. Li and Z. Lin, "Accelerated proximal gradient methods for nonconvex programming," in *Proc. Adv. Neural Inf. Process. Syst.*, 2015, pp. 379-387.
- [68] S. Ghadimi and G. H. Lan, "Accelerated gradient methods for nonconvex nonlinear and stochastic programming," *Mathematical Programming.*, vol. 156, no. 1-2, pp. 59-99, 2016.
- [69] S. Boyd, N. Parikh, E. Chu, *et al.*, "Distributed optimization and statistical learning via the alternative direction method of multipliers," *Found. Trends Math. Learn.*, vol. 3, no. 1, pp. 1-122, 2011.
- [70] N. Parikh and S. Boyd, "Proximal algorithms," *Found. Trends Optim.*, vol. 1, no. 3, pp. 123-231, 2013.